Studies of chain substitution caused sub-fibril level differences in stiffness and ultrastructure of wildtype and *oim/oim* collagen fibers using multifrequency-AFM and molecular modeling

Tao Li [a, 1], Shu-Wei Chang [b, c], Naiara Rodriguez-Florez [d], Markus J. Buehler [c], Sandra Shefelbine [e, ***], Ming Dao [f, **], Kaiyang Zeng [a, *]

[a] Department of Mechanical Engineering, National University of Singapore, Singapore
[b] Department of Civil Engineering, National Taiwan University, Taipei 10617, Taiwan
[c] Department of Civil and Environmental Engineering, Massachusetts Institute of Technology, Cambridge, MA, USA
[d] Department of Bioengineering, Imperial College London, London SW7 2AZ, UK
[e] Department of Mechanical and Industrial Engineering, Northeastern University, Boston, MA, USA
[f] Department of Materials Science and Engineering, Massachusetts Institute of Technology, Cambridge, MA, USA

ARTICLE INFO

ABSTRACT

Molecular alteration in type I collagen, i.e., substituting the α2 chain with α1 chain in tropocollagen molecule, can cause osteogenesis imperfecta (OI), a brittle bone disease, which can be represented by a mouse model (*oim/oim*). In this work, we use dual-frequency Atomic Force Microscopy (AFM) and incorporated with molecular modeling to quantify the ultrastructure and stiffness of the individual native collagen fibers from wildtype (+/+) and *oim/oim* diseased mice humeri. Our work presents direct experimental evidences that the +/+ fibers have highly organized and compact ultrastructure and corresponding ordered stiffness distribution. In contrast, *oim/oim* fibers have ordered but loosely packed ultrastructure with uncorrelated stiffness distribution, as well as local defects. The molecular model also demonstrates the structural and molecular packing differences between +/+ and *oim/oim* collagens. The molecular mutation significantly altered sub-fibril structure and mechanical property of collagen fibers. This study can give the new insight for the mechanisms and treatment of the brittle bone disease.

© 2016 Elsevier Ltd. All rights reserved.

1. Introduction

Collagen is one of the basic building blocks in the multi-level hierarchical structure of osseous tissues and provides the template for mineralization in the formation of bone. Altered collagen affects the mineralization process that occurs within and around the fibril [1–3], resulting in smaller and disorganized mineral crystals with different chemical composition and quantity [4,5]. Not surprisingly, alterations in collagen have disastrous consequences at the whole bone level. One example is osteogenesis imperfecta (OI or brittle bone disease), which originates from mutations of genes coding for type I collagen [6] and results in extreme skeletal fragility [5,7]. The OI mouse model has been widely used to examine bone properties, and develop treatments [8–14]. In the mouse model (*oim/oim*), in which has phenotypic features similar to moderate to severe human OI [15] but with different mutation origin, the *oim/oim* (−/−) collagen fibers are missing the α2 chain, resulting in homotrimers comprising three α1 chains. In contrast, the wildtype (WT or +/+) collagen molecule comprises two α1 and one α2 chains. The typical hierarchical structures of normal type I collagen from atomic to fibrillar level and the mutated homotrimer are illustrated in Fig. 1. The missing α2 chain in *oim/oim* collagen causes significant structural alterations and mechanical deficits in homozygous bone at all levels of the hierarchy, such as reduced ultimate strength, fracture toughness and modulus at the whole bone level [8,9,16]; increased number of vascular pores [10], and
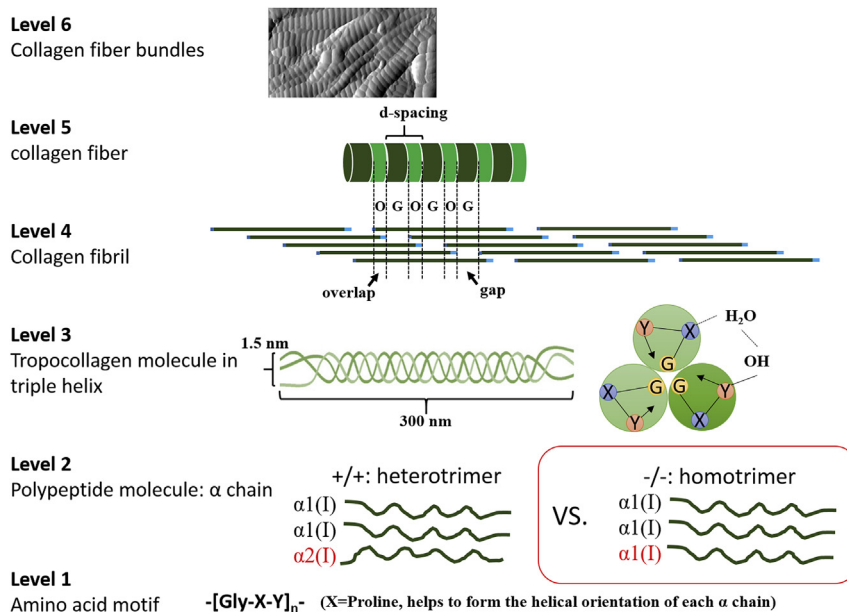

Fig. 1. Schematics of hierarchical structures of normal type I collagen fiber and *oim/oim* homotrimer.

more variable alignment of crystals [17] at the tissue level; stretchier mineralized fibrils [8], altered mineral composition [11], smaller mineral crystals [18], and altered crosslinking [8,19] at the fibril to molecular level. These alterations have been found to result in a loss of mechanical integrity of *oim/oim* bone structure and bone fragility at the tissue and whole bone level. Generally speaking, bones from *oim/oim* can mimic and study the mild to severe human OI features and characteristics [8—14], for example, nano-indentation experiments have showed that the *oim/oim* bone had a lower elastic modulus despite the higher mineralization [9]. Other works also show that the elastic modulus, hardness, carbonate content, and even crystallinity of OI bones have significantly reduced, but the mineral density has increased in the OI bones [20—22]. However, the effects of collagen alterations on mechanical and structural integrity at the fibril and sub-fibril level have not been explored due to the lack of tools with sufficient resolution to probe the basic building blocks of bone.

To understand the mechanisms of molecular mutation induced bone structure and property changes at sub-fibril level, both experimental and theoretical modeling works are needed. For example, AFM (Atomic Force Microscopy) technique together with Fast Fourier Transform (FFT) were widely used to image the collagen morphology and determine the D-space [23—26], on the other hand, Li and colleagues has recently applied AFM to investigate the mechanics of single peptide fibrils [27]. Different from those studies, in this work, we conduct experimental investigations of ultrastructure and properties of mineralized collagen using dual-frequency Atomic Force Microscopy (AFM) technique, which enables the stiffness quantification as well as corresponding morphology observations at nanometer resolution [28,29] and differentiates different compositions [30]. This technique is applied to measure collagen properties at the fibril level (50—100 nm). Such high resolution is attributed to the superior sensitivity of the tip-sample interaction to the material properties due to the higher eigenmode cantilever oscillations in the small amplitude regime [28,31]. Parallel to this, molecular models are developed to explore the underlying structure in the homotrimeric *oim/oim* fibril and heterotrimeric +/+ fibril.

2. Materials and methods

2.1. Animal model

Bone samples used in this study belongs to the B6C3Fe-a/aCol1a2oim/oim strain (*oim/oim*), a mouse model that replicates the moderate to severe condition of OI in humans. These bones were compared to their wildtype controls (+/+) bone samples. The bone samples from those animal model have been previously characterized at whole-bone level, such as the fracture toughness, nanoindentation, tomography (by synchrontron X-ray), *in situ* tensile testing, as well as porosities [9—11].

2.2. Sample preparation

Humeri from two *oim/oim* and two +/+ 8-week old female mice were harvested and cleaned of surrounding soft tissue. The bones were left to dry in air for an hour and embedded in epoxy resin (EPOTHIN; Buehler, Lake Bluff, USA). The epoxy resin and hardener were mixed and let cool for 10 min prior to embedding the bones, in order to increase its viscosity and avoid the infiltration of resin into the pores. The resin-cast bone samples were left to polymerize at room temperature. The embedded humeri were then cut transversally at the mid-diaphysis using a low speed diamond saw (Isomet, Buehler GmbH, Germany). The proximal sections were cut in cubes and polished using increased grades of carbide papers (P800 to P4000). The sections were further polished using alumina powders (0.3 μm and 0.05 μm) to obtain a mirror-like surface for AFM scan. The finished surface has roughness less than 10 nm RMS when observed from 1×1 μm^2 images. Samples were stored under ambient conditions (24 °C and 60% RH) for further AFM characterizations.

2.3. AFM imaging

A commercial AFM system (MFP3D-SA, Asylum Research, USA) was used to conduct all characterization study. The stiffness and sensitivity of the AFM cantilever (PPP-FM, NANOSENSORS, Switzerland) were calibrated using Sader and thermal noise

methods before all imaging. The typical specifications of the cantilevers are listed in Table S1. The entire specimen surface of both *oim/oim* and +/+ bones were firstly scanned by tapping-mode AFM to locate the collagen fibers once for all. In this study, no chemical treatments were used to remove the mineral phase; hence, the collagen fibers were preserved at their native state, i.e. mineralized fibers. The drawback of such preservation is that only limit number of collagen fibers are available for statistical analysis. But in this study, at least tens of fibers were observed and available for the imaging by AFM and dual-frequency AFM methods. A description of dual-frequency AFM method is included in the Supporting Information Note 1.

The D-spacing of collagen fibers was determined using a two dimensional Fast Fourier Transform (2D-FFT) method (Figure S1), which decouples the D-spacing from both the pixel size and fiber orientation [32]. The amplitude AFM images were used to measure the D-spacing of collagen fibers. The area of interest was selected at the straight sections of each fiber, and was undergone 2D-FFT to measure the D-spacing (SPIP software, Image Metrology, Denmark). Thirty-three (33) fibers were measured for each +/+ and *oim/oim* bones. The statistical analysis of D-spacing distributions of collagen fibers was performed using one-way ANOVA method.

2.4. Collagen microfibril modeling

The collagen microfibril model was generated based on the *in situ* structure of full length collagen type I molecule [33] (Protein Data Bank identification code 3HR2), which has a triclinic unit cell ($a \approx 40.0$ Å, $b \approx 27.0$ Å, $c \approx 678$ Å, $\alpha \approx 89.2°$, $\beta \approx 94.6°$, $\gamma \approx 105.6°$). Note that the structure reported in Ref. [34] includes only backbone alpha carbons and the primary sequence of *rattus norvegicus*, therefore, the homology modeling as described in Ref. [35] was used to obtain a full-atomistic structure with the mus collagen sequence. The real sequences of type I α1(I) and type I α2(I) chains of mus musculus (+/+ mouse) were used. The heterotrimer collagen microfibril model was built of two α1(I) chains and one α2(I) chain while the homotrimer collagen microfibril model was built of three α1(I) chains. The sequences were adopted from NCBI protein database (http://www.ncbi.nlm.nih.gov/protein): AAH50014.1 for α1(I) chain and NP_031769.2 for α2(I) chain. In both collagen microfibril models, ions were added to neutralize the system. Full atomistic simulations were performed using modeling code LAMMPS [36] (http://lammps.sandia.gov/) and the CHARMM force field [37] that includes parameters for hydroxyproline amino acids based on a model put forth by Anderson (http://search.library.utoronto.ca/details?6077393&uuid=8d2a6e27-c600-4e13-9555-b25f07b783c9) [38]. An energy minimization using a conjugate gradient scheme was performed before molecular dynamics simulations. Rigid bonds were used to constrain covalent bond lengths and an integration time step of 1 fs is used. Nonbonding interactions were computed using a cut-off for neighbor list at 13.5 Å, with a switching function between 10 and 12 Å for van der Waals interactions. The electrostatic interactions were modeled by the *ewald/n* style, which performs standard coulombic Ewald summations in a more efficient manner [39]. After energy minimization, the collagen molecule was simulated through 5 ns at a constant temperature of 310 K in molecular dynamics simulations to obtain an equilibrium structure.

3. Results

The collagen fibers are in the native air-dried mineralized condition from transverse sections of finely polished mice humeri mounted in the epoxy resin. Usually collagen fibers run perpendicular to this surface, but the fibers may be displaced by mechanical polishing and piled near the bone/resin boundaries. The diameter of *oim/oim* collagen fibers was found to be about half of that of +/+ fibers (Fig. 2A and B). The mean D-spacing (*i.e.,* the repeated gap/overlap banding pattern from the quarter staggered arrangement of collagen molecules) of *oim/oim* fibers (65.70 ± 2.83 nm) is significantly smaller than that of the +/+ fibers (68.19 ± 3.42 nm, $p = 0.002$) (Fig. 2C, D and E). The *oim/oim* fibers also exhibit smaller standard deviation in D-spacing distribution, which indicates reduced heterogeneity. Within each D-spacing unit, the *oim/oim* fibers show a wider gap zone and narrower overlap zone compared to those of the +/+ collagen fibers. Detail statistical analysis of these morphology features is included in Supporting Information Note 2.

To compare with experimental findings we conduct full atomistic molecular modeling of +/+ and *oim/oim* collagen fibers. The model revealed the same structural observations: larger D-spacing and smaller gap/overlap ratio of +/+ collagen fibril than that of *oim/oim* one (Fig. 3). More importantly, the model shows that replacement of the α2 chain with α1 chain alters the structure of the collagen at the molecular level and these alterations lead to a less dense packing of the *oim/oim* collagen fibril. Although both the +/+ and *oim/oim* collagen molecules have the same length, the *oim/oim* collagen molecule has shorter end-to-end distance, which indicates shorter persistence length (bending stiffness/k_BT, where k_B is the Boltzmann constant, and T is the temperature) and thus smaller bending stiffness. The *oim/oim* collagen forms more kinks compared to the +/+ collagen (Fig. 3 and Fig. S2), which agrees with previous study [40]. These kinks affect the packing of collagen molecules at the fibril level, resulting in a fibril with larger lateral spacing and larger gap/overlap ratio, and eventually makes the packing of *oim/oim* collagen fiber looser. On the other hand, Fig. 3 and Fig. S2 actually illustrate the differences between the structure and morphology of the *oim/oim* and +/+ collagens. For example, the collagens in +/+ bone is more straight and with regular D-spacing, but the *oim/oim* collagens show more curling structure, more kink and reduced D-spacing, hence those factors will contribute to the reduction of the mechanical properties in the *oim/oim* bones.

The different mechanical properties between +/+ and *oim/oim* collagen fibers were clearly revealed from the contact stiffness (k^c) mappings. k^c was calculated from the measured contact resonance frequency (f_c) data together with the calibrated AFM cantilever stiffness (k) and free resonance frequency (f_0). According to the cantilever dynamics, $k^c \approx 2kf_c/f_0$, where k and f_0 corresponds to the cantilever eigenmode (3rd used in this study). Larger k^c indicates higher elastic modulus. More detailed description of the method is included in Supporting Information Note 1. Fig. 4A and B shows direct correlation between k^c and morphology of +/+ collagen fibers. The narrow trench (expected to be gap zone) is generally stiffer than the wide protrusion (overlap zone). The dramatically low stiffness along the side walls (dark purple color) of fibers may be due to the slippery tip-fiber contact, thus the analyses were confined in the central region along the fiber axial direction. The stiffness profile and the corresponding height profile were plotted together along the line a-b (Fig. 4C). The profiles of averaged stiffness across the fiber width (~88 nm) were plotted inside a periodic unit with gap and overlap zones identified (Fig. 4D and E). It clearly demonstrates that the stiffness maxima are at the gap zone, whereas the minima are at the gap/overlap boundary. The spatial stiffness variations can be clearly visualized by the first derivative of the stiffness profile (Fig. 4F). The large peaks (± 0.006) indicate sudden stiffness change that located at the height minima with slight offset. Moreover, there are minor peaks (magnitude smaller than 0.002) along the entire fiber, which reveals the stiffness fluctuation within the gap and overlap zones. Such higher order of
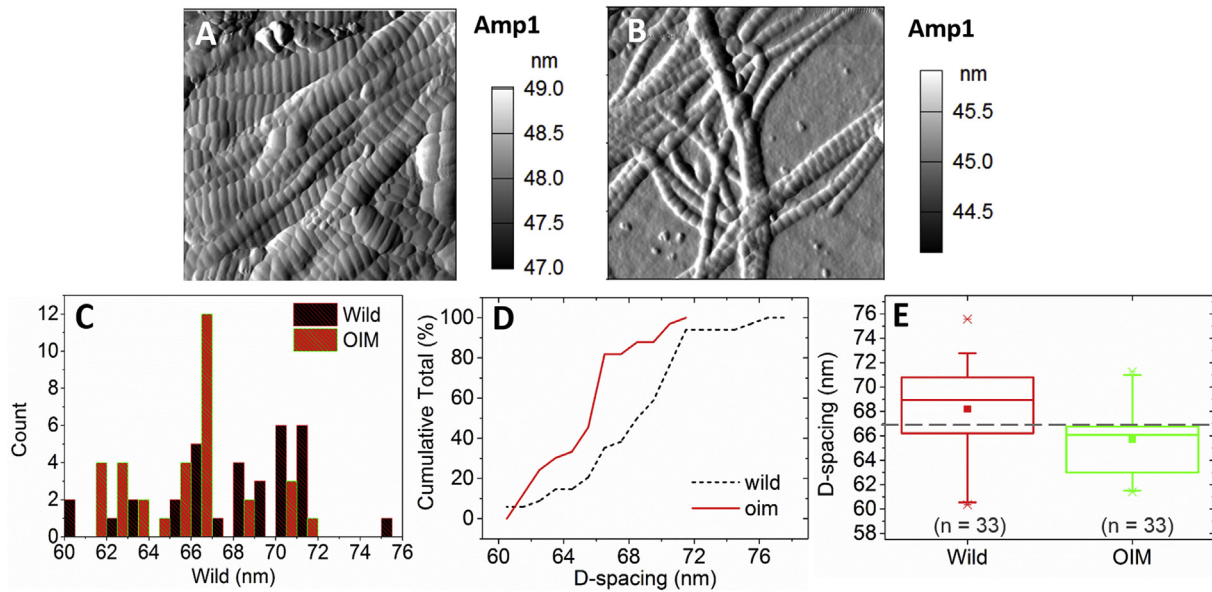
Fig. 2. AFM amplitude images of +/+ collagen fibers (A) and *oim/oim* collagen fibers (B). Scan size is 2 × 2 μm² with 512 × 512 pixels. (C) Histogram of D-spacing distributions of +/+ and *oim/oim* collagen fibers. (D) CDF (cumulative distribution function) of all collagen fibers measured in each group. (E) D-spacing of the +/+ and *oim/oim* collagens. The boxes represent the interquartile range, the crosses represent the data extremes, the whiskers represent the 95% and 5% data range, the square is the mean, the line in the box is the median, and the dashed horizontal line corresponds to the theoretical D-spacing of 67 nm.
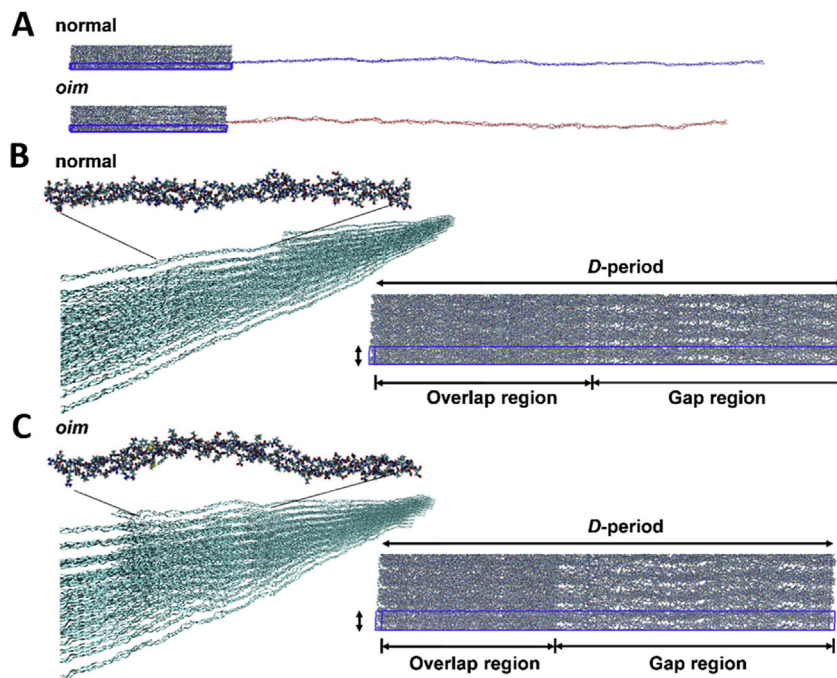

Fig. 3. Molecular modeling of +/+ and *oim/oim* collagen molecules. (A) Molecular structures. The blue box shows the triclinic unit cell of the full atomistic +/+ and *oim/oim* fibrils. (B) and (C) shows the structural differences between +/+ and *oim/oim* collagen at single molecular and fibril levels respectively. (For interpretation of the references to colour in this figure legend, the reader is referred to the web version of this article.)

features are directly demonstrated by small stiffness variations in the overlap zone (Fig. S3). In comparison, the sensitivity of either the amplitude or phase at the fundamental eigenmode (*i.e.* the typical AFM signal) is insufficient to detect detailed property changes within individual gap and overlap zones (Fig. S4). TEM images of stained mineralized collagen fibers showed substructural features within both the gap and overlap zones that reflected the underlying amino acid residues in collagen fibers

[41,42]. The variations in the k^c contrast and stiffness profile may indicate these compositional differences. The stiffness variation along single +/+ fibers follow well-regulated patterns in the gap and overlap zones, similar to those in Fig. 4D and E. Therefore, the organized ultrastructure and the corresponding periodic stiffness variation along +/+ collagen fibers indicate that the mineralization is well controlled by the heterotrimer molecules.

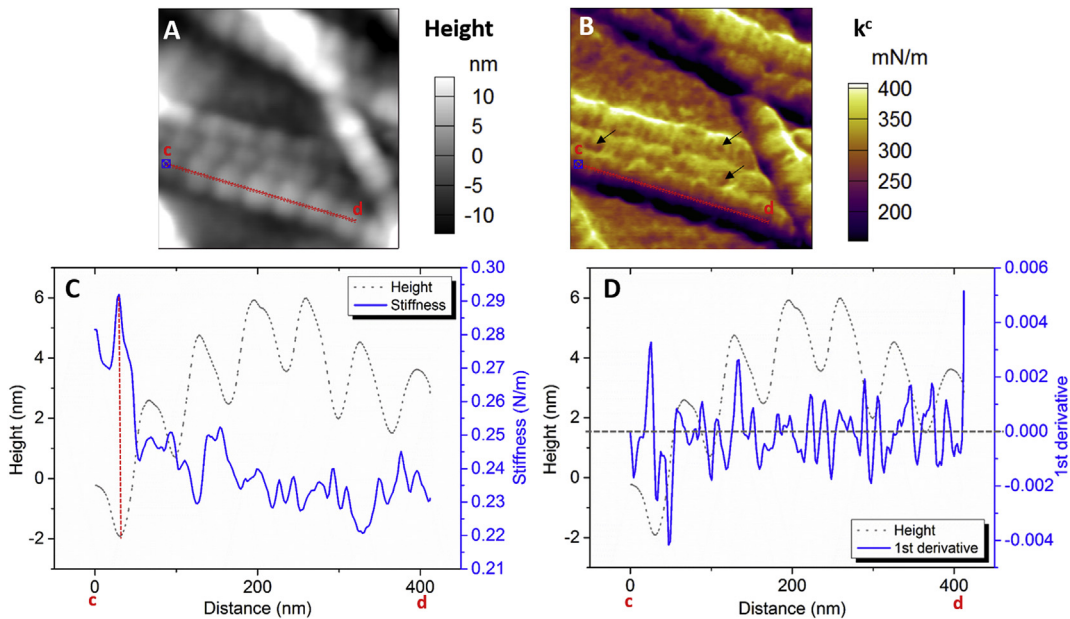The *oim/oim* collagen fibers also had organized periodic units
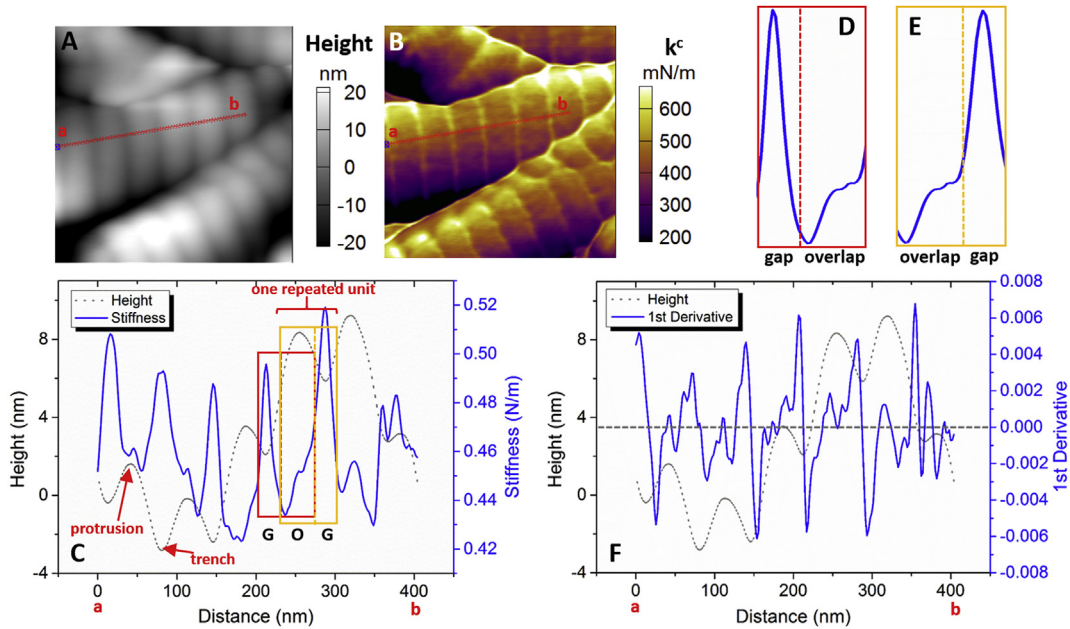
Fig. 4. Dual frequency-AFM images of +/+ collagen fibers (0.5 × 0.5 μm², 256 × 256 pixels). (A) Topography. (B) Stiffness mapping. (C) Stiffness profile along the line a-b with corresponding height profile. The gap and overlap boundaries are identified by the locations with half of the maximum height. (D) Stiffness profile within a periodic unit demonstrates the minimum stiffness at the gap-to-overlap boundary, and largely increased stiffness at the overlap-to-gap boundary (E). (F) First derivative of stiffness profile indicates the locations of sudden stiffness changes along the fiber. The results clearly revealed the periodicity with corresponding well-regulated stiffness fluctuation along the +/+ collagen fiber.

(Fig. 5A), but non-periodic stiffness distribution (Fig. 5B). It was common to have multiple locations with relatively low stiffness (defected points that pointed by arrows in Fig. 5B), which were rarely seen on +/+ ones. The stiffness profile fluctuated randomly (Fig. 5C), without the periodic maxima and minima as those in the +/+ fibers. There was no correlation between stiffness and height profiles. The *oim/oim* collagen fibers also exhibit significantly lower mean stiffness (statistical value averaged over many fibers) and

smaller standard deviation than those of the +/+ ones (Fig. 6). The mean stiffness (Fig. 6A) of +/+ and *oim/oim* collagen fibers is about 0.32 and 0.18 N/m respectively by Gaussian fitting. The CDF curve (Fig. 6B) of the *oim/oim* collagen is entirely on the left-hand-side of the +/+ one, which indicates overall lower stiffness of the *oim/oim* collagen. The K-S test of the CDF curves also indicates that the +/+ collagen is significantly stiffer than that of the *oim/oim* collagen (p < 0.001). Moreover, +/+ collage fibers also show wider stiffness

Fig. 5. Dual-frequency AFM images of oim/oim collagen fibers (0.5 × 0.5 μm², 256 × 256 pixels). (A) Topography. (B) Stiffness mapping. (C) Stiffness data profile along the line c-d with corresponding topography profile. (D) First derivative of stiffness profile indicates the locations of stiffness changes along the fiber. The results showed the organized periodic pattern of oim/oim collagen fiber, but no correlation to the stiffness distribution. The stiffness fluctuates randomly along the fiber, without any recognized repeated pattern.
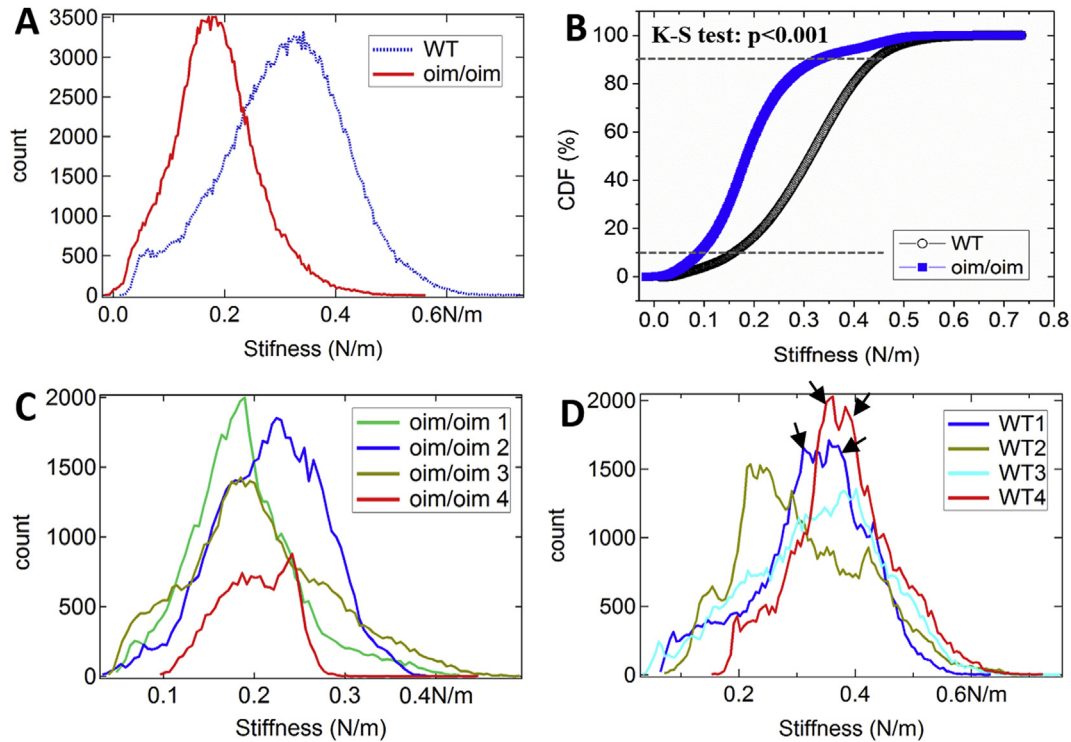
Fig. 6. Stiffness comparison between the +/+ and *oim/oim* collagen fibers. (A) Histograms from 2 × 2 µm² stiffness images (Figs. S6A and E). (B) CDF chart of the histogram presented in (A). (C) and (D) Histograms from 0.5 × 0.5 µm stiffness images of *oim/oim* and +/+ collagen fibers, respectively. The original stiffness images are presented in Figs. S6B—D for +/+ collagen fibers, and Figs. S6F—H for *oim/oim* collagen fibers.

distribution. About 80% of the tested *oim/oim* fibers show stiffness within the range of 0.1—0.3 N/m (Fig. 6C), while for +/+ fibers it is within the range of 0.15—0.45 N/m (Fig. 6D). In addition, the images used for Fig. 6C and D have scan size of 1/16 of that for Fig. 6A. In this case, the stiffness is averaged over less number of fibers, so that more details can be revealed. The exact mean stiffness and distribution varies from image to image, but still centered near the mean value that observed in the image with larger scale. The histograms of the *oim/oim* fibers only show one peak, whereas the stiffness histograms of +/+ fibers usually show split peaks (pointed by black arrows in Fig. 6D). This feature can be smoothed out when the stiffness is averaged over a large number of fibers. These results provided further evidences for the less heterogeneity of *oim/oim* collagen fibers. The first derivative of the stiffness profile along an *oim/oim* collagen fiber fluctuates within ±0.002 without any recognizable patterns and outstanding peaks (Fig. 5D), indicating that the stiffness variations are gentle and gradual along the entire fiber. Although the majority of *oim/oim* fibers showed irregular stiffness variation, some other measured *oim/oim* fibers also showed relatively more regular patterns (Fig. S5). Thus, the *oim/oim* mice bones may comprise both highly and mildly defective collagen fibers. Our model also showed that the overlap region of *oim/oim* collagen molecule has larger lateral spacing between the collagen molecules than that of the +/+ molecule. Thus, the mineralization may also occur at the overlaps and lead to less difference of the stiffness comparing to the gap region. In contrast, for +/+ collagen molecule, much less space is available for mineralization in the overlap zone than in the gap zone because the molecules are more densely packed. Thus, it is unlikely the mineral can grow large at the overlap zone. The preference of crystal mineralization at the gap zone results in a clear periodic stiffness distribution. It is also supported by the previous study that the hydroxyapatite crystals primarily reside in the gap region even at different mineralization stages [43].

4. Discussions

The structures of both +/+ and *oim/oim* collagen fibers are composed by periodic units. The *oim/oim* collagen fibers have a smaller diameter and D-spacing than those of the +/+ fibers. It was reported that the volume fraction of water in *oim/oim* collagen is about ~5% higher than that in +/+ one based on equal amount of collagen molecules, and leads to an increment of interaxial separation between collagen molecule by 1.4 Å [44]. However, based on the fiber diameter that we observed, the volume of *oim/oim* collagen fiber is about 50% less than that of +/+ collagen. Such large volume difference cannot be mainly attributed to the moisture content. On the other hand, the intra- and inter-fibrillar minerals inside a collagen fiber may change the fiber morphology extensively [45]. The fiber diameter might be expanded by the embedded mineral crystals [41]. Thus, the highly organized mineral crystals of the +/+ collagen fiber may contribute to its larger diameter, comparing to the randomly located small size minerals inside *oim/oim* collagen fiber [9]. Thus, the dramatic difference in fiber diameter between the +/+ and *oim/oim* collagen should be attributed to both the different collagen fibrillar organization and collagen-guided mineralization.

The +/+ collagen fibers showed distinctive stiffness profiles recognized in a single periodic unit. The high stiffness peaks are expected to associate with high mineral density. Different terminals of triple helix molecules, *i.e.*, the C- and N-terminal (Fig. 1, GOG units), locate at alternative gap/overlap boundaries. C-terminal is the preferred site for mineral nucleation due to the electrostatic charge attraction [41] and the readily available void space near C-terminal within the mineralized collagen fibril [43]. Therefore, minerals are mostly deposited in the gap zone, which is in accordance with the observed highest stiffness in the gap zone in this work. Such conformation can stiffen the collagen triple helix and

increase the elastic spring constant [46]. In contrast, the *oim/oim* collagen fibers show much lower stiffness. Molecular models, including this study, showed that the *oim/oim* molecules have large kinks, resulting in loosely packed lateral spacing [40], and computational models showed that the homotrimers had a lower intermolecular adhesion force [40,47]. These may contribute to the reduced stiffness in *oim/oim* collagen fibers [9,10,47]. In addition, the stiffness distribution varied randomly along the *oim/oim* fiber with no apparent relationships to the fiber morphology. It implies that the irregular packing and cross-linking associated with the homotrimers may lead to poorly organized mineralization inside the fiber, causing less ordered distribution of the mineral crystals [34] and potential defects with low stiffness as indicated by the dark spots in Fig. 5B. These defects may be originated from the localized glycine mutation that showing reduced stiffness as predicted in the atomic simulation [48]. Such molecular level mutation can affect the fibril mechanical properties in a way of altered stress distribution within fibrils [49]. In general, the *oim/oim* fibers are generally statistically less stiff than the +/+ fibers. Although the morphology may be qualitatively similar between +/+ and *oim/oim* collagen fibers, different mineralization mechanisms initiated by the homotrimer and heterotrimer molecules are reflected by the distinctive stiffness variations along the fibers.

Besides the periodic structure and stiffness distribution, another feature of +/+ collagen is the ordered nanoscale heterogeneity. Higher nanoscale heterogeneity was proposed to contribute to limiting damage growth and enhancing energy dissipation for better toughness at the tissue level [50,51]. Compared with the *oim/oim* collagen fibers, the +/+ collagen fibers show higher heterogeneity in terms of D-spacing and diameter, single fiber stiffness, and average stiffness. These observations are also consistent with the 30% increase in non-enzymatic crosslinks (spatially nonspecific) found in *oim/oim* collagen fibers [10]. Instead of highly-orientated large platelet-like crystals in +/+ bone, the mineral crystals in *oim/oim* bones are less organized, with smaller size [9,52] and low crystallinity [17]. Because the crystals are less ordered spatially (i.e. more evenly distributed throughout the fibril), the stiffness along the fibril does not vary much, which results in a more uniform overall stiffness of the fiber and low heterogeneity. In addition, larger gap spacing in *oim/oim* collagen fibers means that more space is available for the mineral to nucleate and grow, but more mineral contents may not indicate high stiffness at the tissue level [9]. Stiffness may depend more on the quality and organization of mineral crystals, so that the matrix-mediated ordered hierarchical mineral packing inside +/+ bone may dominate over the mineral content and lead to better mechanical performance.

Generally speaking, mineral is responsible for the strength and support of tissue, while the collagen fiber matrix has the role to provide resilience. For *oim/oim* fibers, they are likely to be intrinsically more fragile because of the loose packing, low intermolecular force, small diameter, low average stiffness and also contain local defects that may become highly stressed points under external loading. The deteriorated structural integrity and mechanical property at the fibril level may well be a critical starting point for catastrophic mechanical failure at the tissue level. The full atomistic model used in the present study has provided further insights and quantitative evaluations of different nanoscopic factors involved.

5. Conclusions

In conclusion, this study has presented, for the first time, the significant and unambiguous discrepancies in ultrastructure and stiffness distribution between individual +/+ and *oim/oim* collagen fiber at the sub-fibril level, via analyzing the nanoscale resolution morphology and stiffness images generated by dual-frequency AFM method. For +/+ collagen, the stiffness variation along a single fiber is closely related to the morphology that showing highly regulated periodic pattern, and distinctive stiffness patterns are well maintained at the gap and overlap zones respectively. For *oim/oim* collagen fiber, the defected molecular packing leads to the smaller diameter and D-spacing than those of +/+ collagen. The stiffness fluctuates irregularly along the length of the fiber, and usually has no direct relation to the fiber morphology. The *oim/oim* fibers also exhibit reduced heterogeneity in term of morphology and stiffness. These observations have brought more insights into the relationship between the structure, mechanical property and mineralization of +/+ and *oim/oim* collagen fibers at fibril and sub-fibril level, and also implicate the collagen fiber initiated mechanical failure at the bone level.

Acknowledgements

Appendix A. Supplementary data

Supplementary data related to this article can be found at http://dx.doi.org/10.1016/j.biomaterials.2016.08.038.

References

[1] N. Fratzl-Zelman, R. Morello, B. Lee, F. Rauch, F.H. Glorieux, B.M. Misof, et al., CRTAP deficiency leads to abnormally high bone matrix mineralization in a murine model and in children with osteogenesis imperfecta type VII, Bone 46 (2010) 820—826.

[2] A. Forlino, W.A. Cabral, A.M. Barnes, J.C. Marini, New perspectives on osteogenesis imperfecta, Nat. Rev. Endocrinol. 7 (2011) 540—557.

[3] P. Chavassieux, E. Seeman, P.D. Delmas, Insights into material and structural basis of bone fragility from diseases associated with fractures: how determinants of the biomechanical properties of bone are compromised by disease, Endocr. Rev. 28 (2007) 151—164.

[4] R.D. Blank, A.L. Boskey, Genetic collagen diseases: influence of collagen mutations on structure and mechanical behavior, in: P. Fratzl (Ed.), Collagen: Structure and Mechanics, Springer, US, Boston, 2008, pp. 447—474.

[5] N.P. Camacho, L. Hou, T.R. Toledano, W.A. Ilg, C.F. Brayton, C.L. Raggio, et al., The material basis for reduced mechanical properties in oim mice bones, J. Bone Min. Res. 14 (1999) 264—272.

[6] F.S. Van Dijk, D.O. Sillence, Osteogenesis imperfecta: clinical diagnosis, nomenclature and severity assessment, Am. J. Med. Genet. A 164 (2014) 1470—1481.

[7] J.P. Cassella, P. Barber, A.C. Catterall, S.Y. Ali, A morphometric analysis of osteoid collagen fibril diameter in osteogenesis imperfecta, Bone 15 (1994) 329—334.

[8] A. Carriero, E.A. Zimmermann, A. Paluszny, S.Y. Tang, H. Bale, B. Busse, et al., How tough is brittle bone? Investigating osteogenesis imperfecta in mouse bone, J. Bone Min. Res. 29 (2014) 1392—1401.

[9] M. Vanleene, A. Porter, P.-V. Guillot, A. Boyde, M. Oyen, S. Shefelbine, Ultrastructural defects cause low bone matrix stiffness despite high mineralization in osteogenesis imperfecta mice, Bone 50 (2012) 1317—1323.

[10] A. Carriero, M. Doube, M. Vogt, B. Busse, J. Zustin, A. Levchuk, et al., Altered lacunar and vascular porosity in osteogenesis imperfecta mouse bone as revealed by synchrotron tomography contributes to bone fragility, Bone 61 (2014) 116—124.

[11] M. Vanleene, Z. Saldanha, K.L. Cloyd, G. Jell, G. Bou-Gharios, J.H. Bassett, et al., Transplantation of human fetal blood stem cells in the osteogenesis imperfecta mouse leads to improvement in multiscale tissue properties, Blood 117 (2011) 1053—1060.

[12] J. Saban, M.A. Zussman, R. Havey, A.G. Patwardhan, G.B. Schneider, D. King, Heterozygous oim mice exhibit a mild form of osteogenesis imperfecta, Bone 19 (1996) 575–579.

[13] S.D. Chipman, H.O. Sweet, D.J. McBride, M.T. Davisson, S.C. Marks, A.R. Shuldiner, et al., Defective proα2(I) collagen synthesis in a recessive mutation in mice: a model of human osteogenesis imperfecta, Proc. Natl. Acad. Sci. U. S. A. 90 (1993) 1701–1705.

[14] A.C. Nicholls, G. Osse, H.G. Schloon, H.G. Lenard, S. Deak, J.C. Myers, et al., The clinic features of homozygous α2(I) collagen deficient osteogenesis imperfecta, J. Med. Genet. 21 (1984) 257–262.

[15] A.S. Kamoun-Goldrat, M.F. Le Merrer, Animal models of osteogenesis imperfecta and related syndromes, J. Bone Min. Met. 25 (2007) 211–218.

[16] K. Misof, W.J. Landis, K. Klaushofer, P. Fratzl, Collagen from the osteogenesis imperfecta mouse model (oim) shows reduced resistance against tensile stress, J. Clin. InvestInvestig. 100 (1997) 40–45.

[17] P. Fratzl, O. Paris, K. Klaushofer, W.J. Landis, Bone mineralization in an osteogenesis imperfecta mouse model studied by small-angle x-ray scattering, J. Clin. InvestInvestig. 97 (1996) 396–402.

[18] N. Rodriguez-Florez, E. Garcia-Tunon, Q. Mukadam, E. Saiz, K.J. Oldknow, C. Farquharson, et al., An investigation of the mineral in ductile and brittle cortical mouse bone, J. Bone Min. Res. 30 (2015) 786–795.

[19] T.J. Sims, C.A. Miles, A.J. Bailey, N.P. Camacho, Properties of collagen in OIM mouse tissues, Connect. Tissue Res. 44 (2003) 202–205.

[20] C. Albert, J. Jameson, J.M. Toth, P. Smith, G. Harris, Bone properties by nano-indentation in mild and severe osteogenesis imperfecta, Clin. Biomech. 28 (2013) 110–116.

[21] L. Imbert, J.-C. Aurégan, K. Pernelle, T. Hoc, Mechanical and mineral properties of osteogenesis imperfecta human bones at the tissue level, Bone 65 (2014) 18–24.

[22] A. Carrieo, J.L. Bruse, K.J. Oldknow, J.L. Millán, C. Farquharson, S.J. Shefelbine, Reference point indentation is not indicative of whole mouse bone measures of stress intensity fracture toughness, Bone 69 (2014) 174–179.

[23] Z.R. Bart, M.A. Hammond, J.M. Wallace, Multi-scale analysis of bone chemistry, morphology and mechanics in the oim model of osteogenesis imperfecta, Connect. Tissue Res. 55 (2014) 4–8.

[24] J.M. Wallace, B.G. Orr, J.C. Marini, M.M.B. Holl, Nanoscale morphology of Type I collagen is altered in the Brtl mouse model of osteogenesis imperfecta, J. Struct. Biol. 173 (2011) 146–152.

[25] A.D. Kemp, C.C. Harding, W.A. Cabral, J.C. Marini, J.M. Wallace, Effects of tissue hydration on nanoscale structural morphology and mechanics of individual Type I collagen fibrils in the Brtl mouse model of osteogenesis imperfecta, J. Struct. Biol. 180 (2012) 428–438.

[26] M. Fang, E.L. Goldstein, A.S. Turner, C.M. Les, B.G. Orr, G.J. Fisher, et al., Type I collagen d-spacing in fibril bundles of dermis, tendon, and bone: bridging between nano- and micro-level tissue hierarchy, ACS Nano 6 (2012) 9503–9514.

[27] Y. Li, Y. Sun, M. Qin, Y. Cao, W. Wang, Mechanics of single peptide hydro-gelator fibrils, Nanoscale 7 (2015) 5638–5642.

[28] D. Ebeling, S.D. Solares, Bimodal atomic force microscopy driving the higher eigenmode in frequency-modulation mode: implementation, advantages, disadvantages and comparison to the open-loop case, Beilstein J. Nanotechnol. 4 (2013) 198–207.

[29] R. Garcia, E.T. Herruzo, The emergence of multifrequency force microscopy, Nat. Nanotechnol. 7 (2012) 217–226.

[30] D. Kiracofe, A. Raman, D. Yablon, Multiple regimes of operation in bimodal AFM: understanding the energy of cantilever eigenmodes, Beilstein J. Nanotechnol. 4 (2013) 385–393.

[31] S.D. Solares, G. Chawla, Frequency response of higher cantilever eigenmodes in bimodal and trimodal tapping mode atomic force microscopy, Meas. Sci. Technol. 21 (2010) 125502.

[32] J.M. Wallace, Q. Chen, M. Fang, B. Erickson, B.G. Orr, M.M. Banaszak Holl, Type I collagen exists as a distribution of nanoscale morphologies in teeth, bones, and tendons, Langmuir 26 (2010) 7349.

[33] J.P.R.O. Orgel, T.C. Irving, A. Miller, T.J. Wess, Microfibrillar structure of type I collagen in situ, P. Natl. Acad. Sci. U. S. A. 103 (2006) 9001–9005.

[34] W.J. Landis, The strength of a calcified tissue depends in part on the molecular structure and organization of its constituent mineral crystals in their organic matrix, Bone 16 (1995) 533–544.

[35] A. Gautieri, S. Vesentini, A. Redaelli, M.J. Buehler, Hierarchical structure and nanomechanics of collagen microfibrils from the atomistic scale up, Nano Lett. 11 (2011) 757–766.

[36] S. Plimpton, Fast parallel algorithms for short-range molecular dynamics, J. Comput. Phys. 117 (1995) 1–19.

[37] A.D. MacKerell, D. Bashford, M. Bellott, R.L. Dunbrack, J.D. Evanseck, M.J. Field, et al., All-atom empirical potential for molecular modeling and dynamics studies of proteins, J. Phys. Chem. B 102 (1998) 3586–3616.

[38] D. Anderson, Collagen Self-assembly: a Complementary Experimental and Theoretical Perspective, Ph.D Dissertation, University of Toronto, Toronto, Canada, 2006.

[39] P.J. Iñt Veld, A.E. Ismail, G.S. Grest, Application of Ewald summations to long-range dispersion forces, J. Chem. Phys. 127 (2007) 144711.

[40] S.-W. Chang, Sandra J. Shefelbine, Markus J. Buehler, Structural and mechanical differences between collagen homo- and heterotrimers: relevance for the molecular origin of brittle bone disease, Biophys. J. 102 (2012) 640–648.

[41] F. Nudelman, K. Pieterse, A. George, P.H.H. Bomans, H. Friedrich, L.J. Brylka, et al., The role of collagen in bone apatite formation in the presence of hy-droxyapatite nucleation inhibitors, Nat. Mater 9 (2010) 1004–1009.

[42] W.J. Landis, F.H. Silver, Mineral deposition in the extracellular matrices of vertebrate tissues: identification of possible apatite nucleation sites on Type I collagen, Cells Tissues Organs 189 (2008) 20–24.

[43] A.K. Nair, A. Gautieri, S.-W. Chang, M.J. Buehler, Molecular mechanics of mineralized collagen fibrils in bone, Nat. Commun. 4 (2013) 1724.

[44] C.A. Miles, T.J. Sims, N.P. Camacho, A.J. Bailey, The role of the α2 chain in the stabilization of the collagen Type I heterotrimer: a study of the Type I homotrimer in oim mouse tissues, J. Mol. Biol. 321 (2002) 797–805.

[45] M. Balooch, S. Habelitz, J.H. Kinney, G.W. Marshall, S.J. Marshall, Mechanical properties of mineralized collagen fibrils as influenced by demineralization, J. Struct. Biol. 162 (2008) 404–410.

[46] F.H. Silver, J.W. Freeman, I. Horvath, W.J. Landis, Molecular basis for elastic energy storage in mineralized tendon, Biomacromolecules 2 (2001) 750–756.

[47] S.-W. Chang, B.P. Flynn, J.W. Ruberti, M.J. Buehler, Molecular mechanism of force induced stabilization of collagen against enzymatic breakdown, Bio-materials 33 (2012) 3852–3859.

[48] A. Gautieri, S. Vesentini, A. Redaelli, M.J. Buehler, Single molecule effects of osteogenesis imperfecta mutations in tropocollagen protein domains, Prot. Sci. 18 (2009) 161–168.

[49] A. Gautieri, S. Uzel, S. Vesentini, A. Redaelli, M.J. Buehler, Molecular and mesoscale mechanisms of osteogenesis imperfecta disease in collagen fibrils, Biophys. J. 97 (2009) 857–865.

[50] K. Tai, M. Dao, S. Suresh, A. Palazoglu, C. Ortiz, Nanoscale heterogeneity promotes energy dissipation in bone, Nat. Mater 6 (2007) 454–462.

[51] H. Yao, M. Dao, D. Carnelli, K. Tai, C. Ortiz, Size-dependent heterogeneity benefits the mechanical performance of bone, J. Mech. Phys. Solids 59 (2011) 64–74.

[52] B. Grabner, W.J. Landis, P. Roschger, S. Rinnerthaler, H. Peterlik, K. Klaushofer, et al., Age- and genotype-dependence of bone material properties in the osteogenesis imperfecta murine model (oim), Bone 29 (2001) 453–457.